Electron-phonon interaction in Ti_nO_{2n-1} using first-principles calculations

S. Vahid Hosseini,[1] Mohaddeseh Abbasnejad,[2] and Mohammad Reza Mohammadizadeh[1,*]

[1]*Superconductivity Research Laboratory (SRL), Department of Physics, University of Tehran, North Kargar Ave., P. O. Box 14395–547, Tehran, Iran*

[2]*Faculty of Physics, Shahid Bahonar University of Kerman, Kerman, Iran*

(Received 16 August 2021; revised 9 November 2021; accepted 9 November 2021; published 2 December 2021)

In the present study, the electronic, phonon, and electron-phonon interactions of titanium suboxide structures including TiO, Ti_2O_3, Ti_3O_5, Ti_4O_7, and Ti_5O_9 were investigated in the framework of density-functional theory. The mechanism of superconductivity in these materials seems to be phonon mediated, probably with participation of paramagnetic spin fluctuations. The influence of pressure on the superconducting transition temperature (T_C) of cubic TiO and Ti_4O_7 could be explained by this mechanism. Our calculations predict a low T_C of ~3.5 K for Ti_5O_9. It implies that Ti_5O_9 would be a superconductor lying in the weak coupling regime.

DOI: 10.1103/PhysRevB.104.224101

I. INTRODUCTION

Titanium suboxides with generic chemical formula Ti_nO_{2n-1} have drawn much attention in the last decades due to their interesting physical and electronic properties. Recently, it has been reported that Ti_nO_{2n-1} ($n = 1$–4) exhibit low-T_C superconductivity [1–4]. Despite the T_C values being merely on the order of several K, these materials can be fascinating in this area. In contrast to crystalline chemical compounds (i.e., yttrium barium copper oxide) [5], and iron-based superconductors [6], which can be toxic and harmful, titanium suboxides are both environmentally friendly and easy-to-fabricate materials. Hence, finding out the mechanism of superconductivity in these materials can be advantageous. The primary research on electrical resistivity and superconductivity of titanium monoxides (TiO) was done by Hulm *et al.* [7]. TiO at ambient conditions is known to exist either in cubic [8] phase, which contains about 15% of (in principle, disordered) vacancies on both Ti and O sublattices [9], or in a monoclinic phase, which in fact incorporates 1/6 of such vacancies on the underlying cubic lattice in a particular ordered arrangement. In principle, the cubic phase may exist throughout the compositions TiO_x with x varying from 0.75 to 1.30 [8]. It should be noted that the dynamical stability of cubic phase is rigorously dependent upon the presence of vacancies.[1] This subject was studied in our previous work [10] in detail. The electrical properties and superconductivity are strongly affected by the value of x so that the maximum magnitude of superconductivity and conductivity is observed at $x = 1$ [7,11]. Hulm *et al.* [7] reported $T_C \sim 1$ K for the cubic $TiO_{1.07}$. Later, Wang *et al.* [12] could reach $T_C \sim 5.5$ K by setting the exact Ti/O molar ratio of 1:1. In addition, Zhang *et al.* [1] fabricated cubic TiO as a single crystal or epitaxial thin films deposited on Al_2O_3 substrate that helped to achieve the T_C values of ~7.4 K. These latter authors attributed the enhanced superconductivity to the involvement of substrate phonons in the electron-phonon interaction at the TiO-Al_2O_3 interface. Moreover, Zhang *et al.* [1] also pointed out, on the basis of their analysis of scanning transmission electron microscopy results for TiO films, that the inhomogeneous titanium and oxygen stoichiometry may significantly affect the local electronic structure as well as superconductivity for TiO film. Recently, Xu *et al.* [13] have succeeded in enhancing the T_C up to ~11 K for nanoparticles made of TiO core covered with $a \approx$ 5-nm shell of amorphous TiO_{1+x}.

Ti_2O_3 can be fabricated as a single-crystal thin film grown on α-Al_2O_3 at low (high) temperature, to be referred to as Ti_2O_3-LT (Ti_2O_3-HT). Orthorhombic-structured Ti_2O_3-HT, of space group $Immm$, is a superconductor with $T_C \sim 8$ K [3]. Meanwhile, the other polymorph rhombohedral corundumlike Ti_2O_3-LT with space group $R\bar{3}C$ does not show superconductivity. The stronger electron-phonon coupling is reported for the former material relative to the latter one [3], although more studies on the mechanism of superconductivity are needed.

Ti_3O_5 crystallographic data indicate the existence of three different polymorphs for this structure, namely, α-Ti_3O_5 (orthorhombic, anosovitelike, group $Cmcm$) [14], β-Ti_3O_5 (monoclinic, group $C2/m$) [15], and γ-Ti_3O_5 (monoclinic, group $I2/c$) [16]. The first semiconductor-semiconductor phase transition is observed between α- and β-Ti_3O_5 in temperature range 440–460 K. The other phase transition occurs from β- to γ-Ti_3O_5 at temperature ~250 K [17]. The measurements of the valence band and core levels prove that β-Ti_3O_5 develops the energy band gap of ~0.1 eV, while γ-Ti_3O_5 shows a metallic behavior [18]. Recently, Yoshimatsu *et al.* [4] measured $T_C \sim 7.1$ K for γ-Ti_3O_5 thin film with the thickness of ~120 nm deposited on α-Al_2O_3 substrates. They investigated the mechanism of superconductivity

*zadeh@ut.ac.ir

[1]We found that phonon dispersion in cubic TiO at ambient pressure reveals imaginary frequencies over large part of the Brillouin zone; earlier calculations by Andersson *et al.* [58] hint at the same direction. At the same time, the cubic phase with 1/8 sites empty, i.e., $Ti_{7/8}O_{7/8}$ becomes dynamically stable.

on the basis of electrical measurements and electronic phase transition. The electrical resistivity of Ti_3O_5 depends on temperature, as was evidenced through Hall measurements, and is sensitive to the pressure under which the thin film is grown [4]. However, the discussion regarding the origin of superconductivity is still under debate.

Yet another structure in which the superconductivity was observed is Ti_4O_7, the first member of Magnéli phase with space group $P\bar{1}$ [19]. Ti_4O_7 is known to exist in three phases, namely LT, intermediate-temperature (IT), and HT ones. The LT phase (formed in the temperature range of 125–140 K) behaves like a semiconductor for which however different values of band gap have been reported. For instance, data extracted from optical measurements suggest a band gap of 0.25 eV [20], while conductivity and spectroscopy data yield values of 0.04 eV [21] and 0.6 eV [22], respectively. The semiconducting behavior was maintained in IT phase (140–150 K). In both LT and IT phases, there are Ti^{4+}–Ti^{4+} and Ti^{3+}–Ti^{3+} bonds, in which Ti^{3+}–Ti^{3+} form bipolarons. The difference is that some of the bipolaronic bonds are broken in the IT phase compared to the LT phase due to temperature fluctuations. The HT phase, emerging above 150 K, reveals a metallic behavior. This phase contains quite weakened bipolarons and conduction electrons. Primary studies predicted the possibility of superconductivity through bipolarons acting as localized Cooper pairs. These bipolarons can interact via phonons, such that the electron-phonon coupling can be expected in Ti_4O_7 [23]. Following this, Yoshimatsu *et al.* [4] observed the superconducting temperature of about 3 K in Ti_4O_7 thin film deposited on α-Al_2O_3 substrate with thickness of ∼120 nm at 1×10^{-6} Torr. However, they pointed out that the inverse Hall coefficient $(1/R_H)$ measurements in superconducting Ti_4O_7 phase were independent of temperature, indicating no trace of bipolarons states. The absence of bipolarons results in the suppression of the insulating states.

Furthermore, the influence of pressure on T_C of Ti_4O_7 [24] and TiO cubic [1] films was studied to elucidate the mechanism of superconductivity in more detail. The results show that increasing the pressure led to the decrease of T_C by the rate of 0.7 K/GPa (0.5 K/GPa) in the case of Ti_4O_7 (TiO cubic) film. Therefore, it is believed that the strain/stress may affect the electron-phonon interaction inside the materials or through their interfaces.

Although various experimental and theoretical studies have been dedicated to the investigation of superconductivity mechanism in Ti_nO_{2n-1} materials, the comprehensive model has not been presented up to now. In the view of information so far available, these materials can be electron-phonon mediated superconductors. Therefore, the present paper aims to shed light on the mechanism of superconductivity in these structures using first-principles calculations. In short, we address the following issues: (i) electronic and phonon properties of Ti_nO_{2n-1} $(n = 1–5)$, (ii) mechanism of superconductivity in Ti_nO_{2n-1} structures, (iii) verification whether the proposed mechanism could account for the experimental superconducting temperatures of Ti_nO_{2n-1} $(n = 1–4)$, and (iv) prediction of the superconducting temperature of Ti_5O_9.

The methodology and computational details based on density-functional (perturbation) theory (DFT/DFPT) are presented in the next part. Then, the results including electronic and phonon properties as well as the superconductivity mechanism based on electron-phonon interactions (EPIs) are discussed. Finally, the conclusions are drawn. Understanding the superconductivity mechanism can open a path for improving the superconductivity properties in these materials.

II. METHODS AND TECHNICALITIES

To include EPIs in the framework of DFT, the Kohn-Sham potential $V_{SCF}(\mathbf{r}, \boldsymbol{\tau})$ is expanded in terms of nuclei displacement u (in one direction for simplicity) as

$$V_{SCF}(\mathbf{r};\tau) = V_{SCF}(\mathbf{r};\tau_0) + \frac{\partial V_{SCF}}{\partial \tau}u + \frac{1}{2}\frac{\partial^2 V_{SCF}}{\partial^2 \tau}u^2 + ..., \tag{1}$$

where $\mathbf{r}$ and $\boldsymbol{\tau}$ are the position of electrons and ions, respectively, and τ_0 marks the equilibrium structure. The first term denotes the Kohn-Sham potential for the clamped nucleus, and the higher-order derivative terms are indicative of perturbed Hamiltonian leading to EPIs.

Following this, a variation of Kohn-Sham potential introduces the electron-phonon matrix elements $[g_{mnv}(\mathbf{k}, \mathbf{q})]$ as [25]

$$g_{mnv}(\mathbf{k}, \mathbf{q}) = \langle u_{m\boldsymbol{k}+\boldsymbol{q}} | \Delta_{qv} V_{SCF} | u_{n\boldsymbol{k}} \rangle_{occ.}, \tag{2}$$

where $u_{n\boldsymbol{k}}$ and $u_{m\boldsymbol{k}+\boldsymbol{q}}$ are lattice-periodic parts of the Bloch wave function characterized by the crystal momenta $\boldsymbol{k}$ and $\boldsymbol{k}+\boldsymbol{q}$ in the bands n and m, respectively. The Fourier transformation of the perturbed Kohn-Sham potential $(\Delta_{qv} V_{SCF})$ can be expressed as [25]

$$\Delta_{qv} V_{SCF} = \sum_{\kappa\alpha p} e^{-i\boldsymbol{q}\cdot(\boldsymbol{r}-\boldsymbol{R}_p)} \sqrt{\frac{\hbar}{2M_\kappa \omega_{\boldsymbol{q}v}}}\, e_{k\alpha,\, v}(\boldsymbol{q})\, \frac{\partial V_{SCF}(\mathbf{r})}{\partial \tau_{\kappa\alpha p}}, \tag{3}$$

where κ numbers the ions in the unit cell, α is the Cartesian direction, $\boldsymbol{q}$ is the phonon wave vector, p the index of unit cell located at the lattice vector $\boldsymbol{R}_p$, M_κ the mass of the nucleus κ, $\hbar$ the reduced Planck constant, $\omega_{\boldsymbol{q}v}$ the phonon frequency at momentum $\boldsymbol{q}$ and band index v, and $e_{k\alpha,\, v}(\boldsymbol{q})$ is the phonon polarization. Using the DFPT technique, the variation of V_{SCF} in Eq. (3) can be attained iteratively. Having electron-phonon matrix elements through Eq. (2), the properties of superconductivity can be determined.

The first property is the electron-phonon coupling constant (λ), which describes the strength of EPIs in the metallic materials that is written as [25]

$$\lambda = N_F \left\langle \left\langle \sum_v \frac{|g_{mnv}(\mathbf{k}, \mathbf{q})|^2}{\hbar \omega_{\boldsymbol{q}v}} \right\rangle \right\rangle_{FS}, \tag{4}$$

where N_F is the number of electrons at the Fermi surface and $\langle\langle \ldots \rangle\rangle_{FS}$ is the average over all possible combinations with $\epsilon_{n\boldsymbol{k}}$ and $\epsilon_{m\boldsymbol{k}+\boldsymbol{q}}$ on the Fermi surface. The quantity λ is dimensionless and typically ranges between 0 and 2 [25].

In Bardeen-Cooper-Schrieffer (BCS) theory, T_C is proportional to $\exp(-1/\lambda)$. This quantity can be estimated semiempirically, using, e.g., the McMillan formula [26], later refined by Allen and Dynes [27], leading to an expression

$$T_C = \frac{\omega_{\log}}{1.2} \exp\left(-\frac{1.04(1+\lambda)}{\lambda - \mu_c^*(1+0.62\lambda)} \right), \tag{5}$$

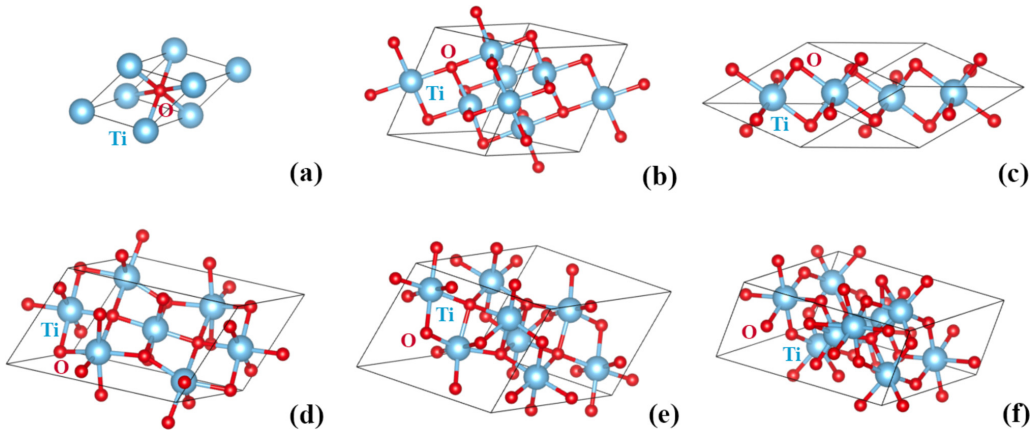

FIG. 1. The overal view of primitive unit cells for (a) c-TiO, (b) m-TiO, (c) Ti_2O_3-HT, (d) γ-Ti_3O_5, (e) Ti_4O_7, and (f) Ti_5O_9.

in which $\omega_{\log}$ is a logarithmic average of the phonon frequency, and $\mu_c{}^*$ is the Coulomb pseudopotential which can be typically set between 0.1 and 0.2 [25].

In many applications, the Eliashberg spectral function $\alpha^2F(\omega)$ is introduced to count the electron-phonon scattering from states with given energy $\epsilon_{n\boldsymbol{k}}$ into states with $\epsilon_{m\boldsymbol{k}+\boldsymbol{q}}$, irrespective of their momenta. This function can be defined as a product of an effective electron-phonon coupling and phonon density of states. Hence, this function gives the coupling between an initial state and all the other states on the Fermi surface differing energetically from the initial state by phonon energy [25]:

$$\alpha^2F(\omega) = \frac{1}{N_F}\sum_{mnv,\,\boldsymbol{k}\mathbf{q}} |g_{mnv}(\mathbf{k},\,\mathbf{q})|^2\delta(\epsilon_{n\boldsymbol{k}})\delta(\epsilon_{m\boldsymbol{k}+\boldsymbol{q}}) \times\ \delta(\omega-\omega_{\boldsymbol{q}v}). \tag{6}$$

The Eliashberg spectral function is dimensionless, as is the electron-phonon coupling constant. Using isotropic approximation, one can express λ and $\omega_{\log}$ in terms of Eliashberg spectral function as follows [28]:

$$\lambda = 2\int_0^{\omega}\frac{\alpha^2F(\omega)}{\omega}\,d\omega, \tag{7}$$

$$\omega_{\log} = 2\int_0^{\omega}\frac{\alpha^2F(\omega)}{\omega}\ln\omega\,d\omega. \tag{8}$$

The calculations were performed in the framework of DFPT using the QUANTUM ESPRESSO package [29] with plane-wave basis set. The ultrasoft pseudopotentials included $3s$, $3p$, $3d$, and $4s$ states as valence ones for Ti and $2s$, and $2p$ as valence ones for O. Exchange correlation was treated within the generalized gradient approximation (GGA) with the parametrization by Perdew-Burke-Ernzerhof [30]. The cutoff kinetic energy for the plane-wave expansion [verified by convergence tests for the forces to be stable within 10^{-5}(Ry/a.u.)] was chosen at 45, 42, 58, 60, and 60 Ry for TiO, Ti_2O_3, γ-Ti_3O_5, Ti_4O_7, and Ti_5O_9, respectively. The Brillouin-zone (BZ) integration was performed using $6\times6\times6$ k-space divisions within the Monkhorst-Pack scheme [31]. To calculate the dynamical matrix, the BZ was sampled with a $3\times3\times3$ q-point grid. It was found that these samplings using a Gaussian smearing of 0.05 Ry of delta functions entering in Eq. (6) provide a proper convergence of electron-phonon matrix elements. The results of convergence tests for one of the proposed materials, taken as a typical example, are presented in Appendix A. Prior to such calculation, the geometry optimization was always performed, whereby the coordinates of the atoms were relaxed until the Hellman-Feynman forces were less than 10^{-5} (Ry/a.u.).

III. RESULTS AND DISCUSSION

A. Structural and electronic properties

Figure 1 shows primitive unit cells of Ti_nO_{2n-1} ($n=1$–5). Cubic TiO, as already discussed, possesses ~15% disordered vacancies in both titanium and oxygen sites. In our previous work [10], it was acknowledged that the pure cubic TiO shows dynamical instability. As a simplest way to remedy this instability while maintaining the cubic symmetry, we allowed ordered vacancies at 1/8 sites of both Ti and O sublattices, creating hence a $2\times2\times2$ supercell, the Ti and O vacancies being logically at maximal possible separation. This cubic $Ti_{0.875}O_{0.875}$ structure is referred to as c-TiO in the present work. The conventional unit cell of the monoclinic TiO, labeled as m-TiO, nominally presents 12 titanium and 12 oxygen sites, of which two of each species are vacant [9]. Ti_2O_3-LT is isostructural with Al_2O_3, with approximate hexagonal close packing of the oxygen and titanium in two-thirds of the octahedral sites [32]. In the present work, we focus on physical properties of Ti_2O_3-HT in which the superconductivity has been observed. The electronic, phonon, and electron-phonon properties of Ti_2O_3-LT are provided in Appendix B. γ-Ti_3O_5 stands for a monoclinic structure proposed to be metastable at room temperature, found only in the form of nanocrystals [33]. Ti_4O_7, the first member of Magnéli phase, is triclinic and contains two formula units per unit cell. The Ti_4O_7 structure consists of rutilelike slabs of TiO_6 octahedra extending infinitely in two dimensions, being four octahedra thick in the third direction. As mentioned already, this structure contains LT, IT, and HT phases in which the lattice parameters and the atomic positions were provided by Marezio *et al.* experimentally [19]. In the present work, the HT phase was used in which Ti_4O_7 is metallic. The second member of Magnéli phase, characterized by Andersson [34], is Ti_5O_9 with triclinic symmetry whose unit cell contains two

TABLE I. Optimized crystallographic data, including lattice parameters a, b, c; lattice angle α°, β°, γ°, and equilibrium volume V. The calculations correspond to zero pressure and temperature.

Structure	a (Å)	b (Å)	c (Å)	α°	β°	γ°	V (Å^3)	Error (%)
c-TiO	4.27					90	77.85	6.60
Expt. [8]	4.18					90	73.03	
m-TiO	5.84	9.31	4.16			107° 36′	215.98	0.01
Expt. [9]	5.85	9.34	4.14			107° 32′	215.94	
Ti_2O_3-LT	5.49					55° 07′	103.95	1.04
Expt. [36]	5.43					56° 00′	102.88	
Ti_2O_3-HT	5.16			146° 82′	134° 63′	57° 34′	53.25	−8.60
Expt. [3]	5.37			149° 69′	131° 40′	58° 34′	58.30	
γ-Ti_3O_5	5.05	5.05	7.80	111° 38′	111° 38′	74° 60′	170.76	−0.05
Expt. [4]	5.65	5.65	7.18	109° 58′	109° 58′	53° 28′	170.85	
Ti_4O_7	5.62	6.94	7.16	64° 21′	71° 05′	75° 03′	236.22	1.51
Expt. [19]	5.59	6.91	7.13	64° 09′	71° 12′	75° 47′	232.69	
Ti_5O_9	5.60	7.16	8.94	97.64	112.56	108° 72′	300.66	1.80
Expt. [34]	5.56	7.12	8.86	97.55	112.34	108° 50′	295.32	

Ti_5O_9 formula units. This structure is the same as Ti_4O_7, except that the thickness in the third dimension consists of five TiO_6 octahedra.

Table I shows optimized structure parameters of titanium suboxides. One sees that the error in the volume as compared to the experiment is less than 2%, with the exception of two structures. An elevated deviation in cases of c-TiO and Ti_2O_3-HT can be attributed to the "uncontrollable presence" of vacancies in genuine c-TiO and to the extension of Ti_2O_3 from $TiO_{1.49}$ to $TiO_{1.51}$ [35]. Overall, one can be satisfied with the performance of GGA in what concerns the description of structural parameters in these materials.

The electronic band structures of Ti_nO_{2n-1} ($n = 1$–5) are presented in Fig. 2. The labeling of high-symmetry points over the respective BZ follows Setyawan *et al.* [37]. Some bands cross the Fermi level, indicating the metallic behavior of these compounds. The presence of extremely steep bands, i.e., highly mobile electrons, along with extremely flat bands, i.e., confined conduction electrons around Fermi energy (E_F) in these structures, can enhance electron pairing and affect the superconductivity. For c-TiO, one sees low-dispersive bands near E_F along the Γ-L-U and W-L-K directions, which increase the density of states at E_F.

Moreover, along the Γ-X-W direction, the electronic dispersion of bands which cross the Fermi level is strong. The strong dispersion can also be recognized by mode-resolved electron-phonon coupling. Thus, it can be expected that the electron-phonon coupling is high in these regions. In m-TiO, the degeneracies of "sensitive" bands in Γ are lifted, in contrast to the situation in highly symmetric. In Ti_2O_3-HT, the dispersion of bands crossing the Fermi level is extremely steep. However, a low-dispersive band that can be traced in the Z-Γ direction contributes to enhancing the number of electron states around the Fermi level. This might add to the creation of Cooper pairs provided that the electron-phonon interaction is considerable. Weakly dispersive bands near the Fermi level are also observed along the Y-X_1 direction in case of γ-Ti_3O_5. For Ti_4O_7 and Ti_5O_9, the bands are also rather flat near the Fermi level, however, crossing E_F. The electronic densities of states (DOS) of Ti_nO_{2n-1} are displayed in Fig. 3. For all titanium suboxides, the electronic DOS reveals that energy range between −3 and −8 eV is mostly populated by O-2p orbitals forming the valence bands, whereas the conduction bands are mainly coming from the Ti-3d states. Moreover, an energy interval (p−d gap) with the order of ∼2 eV below the Fermi level occurs between O-2p and Ti-3d bands in all titanium suboxides. In fact, the strong interaction between these orbitals will imply large splitting. The results of calculated DOS for Ti_nO_{2n-1} ($n = 1$–5) are generally consistent with those reported in Refs. [38–43]. It is also interesting to note that in those titanium suboxides which exhibit higher T_C (c-TiO, Ti_2O_3-HT, γ-Ti_3O_5), the Fermi level is situated on the peaks of electronic DOS whereas for the others (m-TiO, Ti_4O_7, and Ti_5O_9), it is in the pseudogap.

The Fermi surface for Ti_nO_{2n-1} ($n = 1$–5) family is displayed in Fig. 4. Each column displays the 3D Fermi surface corresponding to a band (labeled 1, 2, or 3 in Fig. 2) crossing the Fermi level. For c-TiO, the Fermi surface is composed of two different sheets. One of them forms hole pockets around X points whereas the other is a complex sheet formed of electron and hole pockets extended over the entire BZ. For m-TiO, there are three sheets forming the hole pockets around M points, and two elliptical electron pockets extended along the Γ-L direction and L points. For Ti_2O_3-HT, there are three different inhomogeneous sheets leading to the hole pockets around T points, electron pockets in X and X_1 points, and the cuplike electron pockets along the X_1-Z direction. The Fermi surface of γ-Ti_3O_5 is composed of small hole pockets in the Z point, large connected sheets that are a mixture of electron and hole pockets in L and Z points and the small electron pockets in Y points. For the case of Ti_4O_7 and Ti_5O_9, having triclinic symmetry, the Fermi surfaces include quite asymmetrical disconnected sheets. Ti_4O_7 is made up of holelike pockets mainly located at L points and X-Y intersections. The other electronlike sheets come from N-R intersections and corners of X regions, and yet another one, cone-shaped, extends in the Γ

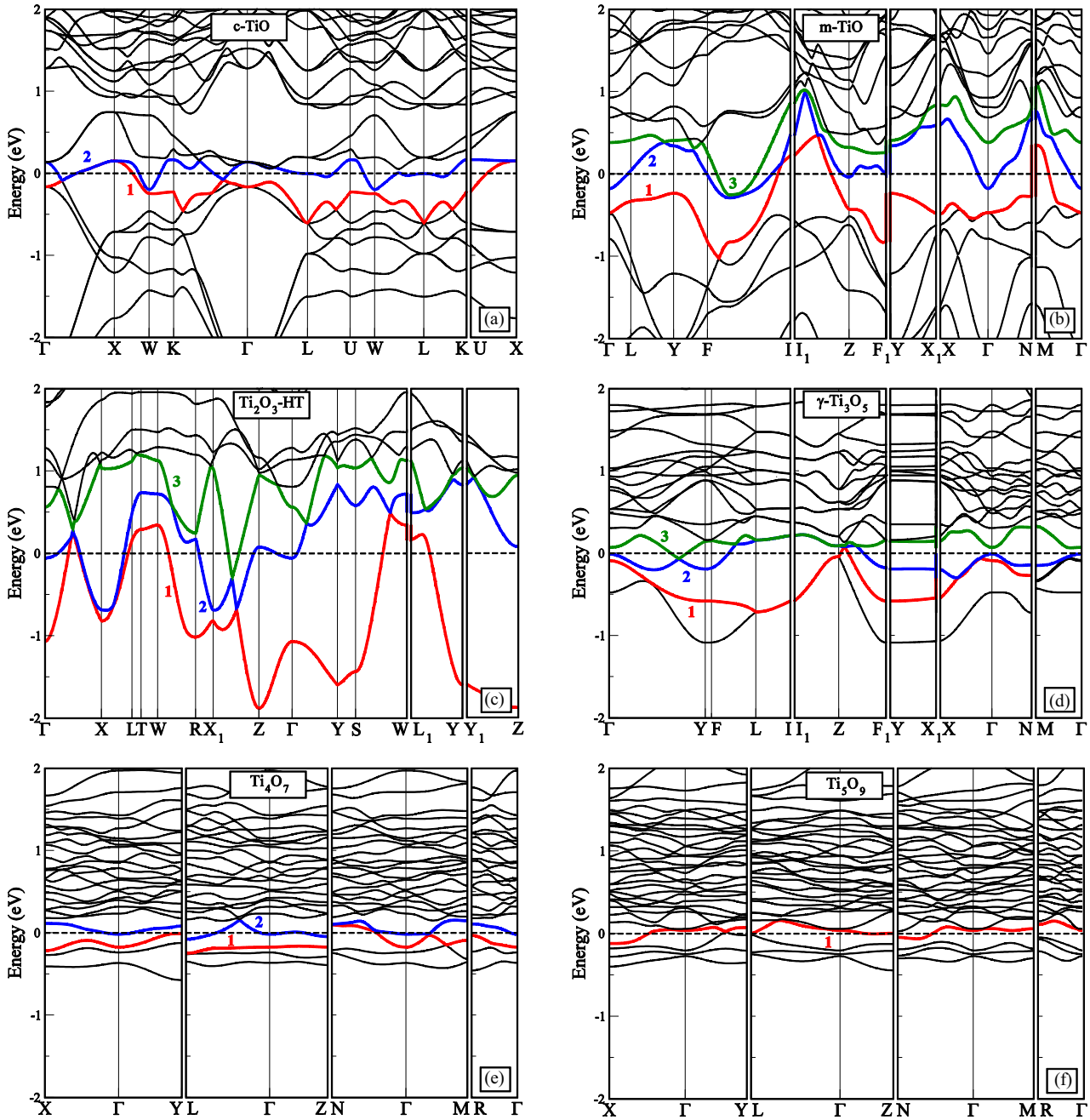

FIG. 2. Electronic band structures for (a) c-TiO, (b) m-TiO, (c) Ti_2O_3-HT, (d) γ-Ti_3O_5, (e) Ti_4O_7, and (f) Ti_5O_9. The dashed line indicates the Fermi energy. The bands crossing the Fermi energy are represented with different colors and numbers.

to Y direction. Finally, for the case of Ti_5O_9 there is only one sheet, a mixture of electron and hole pockets, which are situated around R and N points. In consequence, the existence of 3D different geometry for the electron and holelike sheets in Ti_nO_{2n-1} ($n = 1$–5) suggests that Fermi surface nesting [44] is hardly possible. Thus, building up of charge-density wave phase in Ti_nO_{2n-1} superconductors seems unlikely [45].

B. Lattice-dynamical properties

Figure 5 shows phonon dispersion curves and phonon densities of modes for Ti_nO_{2n-1} ($n = 1$–5). The stability of these structures is confirmed by the absence of any imaginary frequency modes in the whole BZ.

Generally, it is obvious from the phonon dispersion curves of titanium suboxides that the higher modes dominated by oxygen vibrations come out relatively flat. These modes can be identified as rigid-unit modes [46,47], in which TiO octahedra move together as rigid units and thus do not distort the bonds connecting the atoms within the unit. For instance, in m-TiO there are two isolated flat branches at about 550 and 600 cm^{-1} corresponding to localized vibrations along the (shortest) monoclinic b axis [48]. For the cases of Ti_4O_7 and Ti_5O_9 with, respectively, 66 and 84 normal modes, there are many optical flat branches ranging from ∼100 to

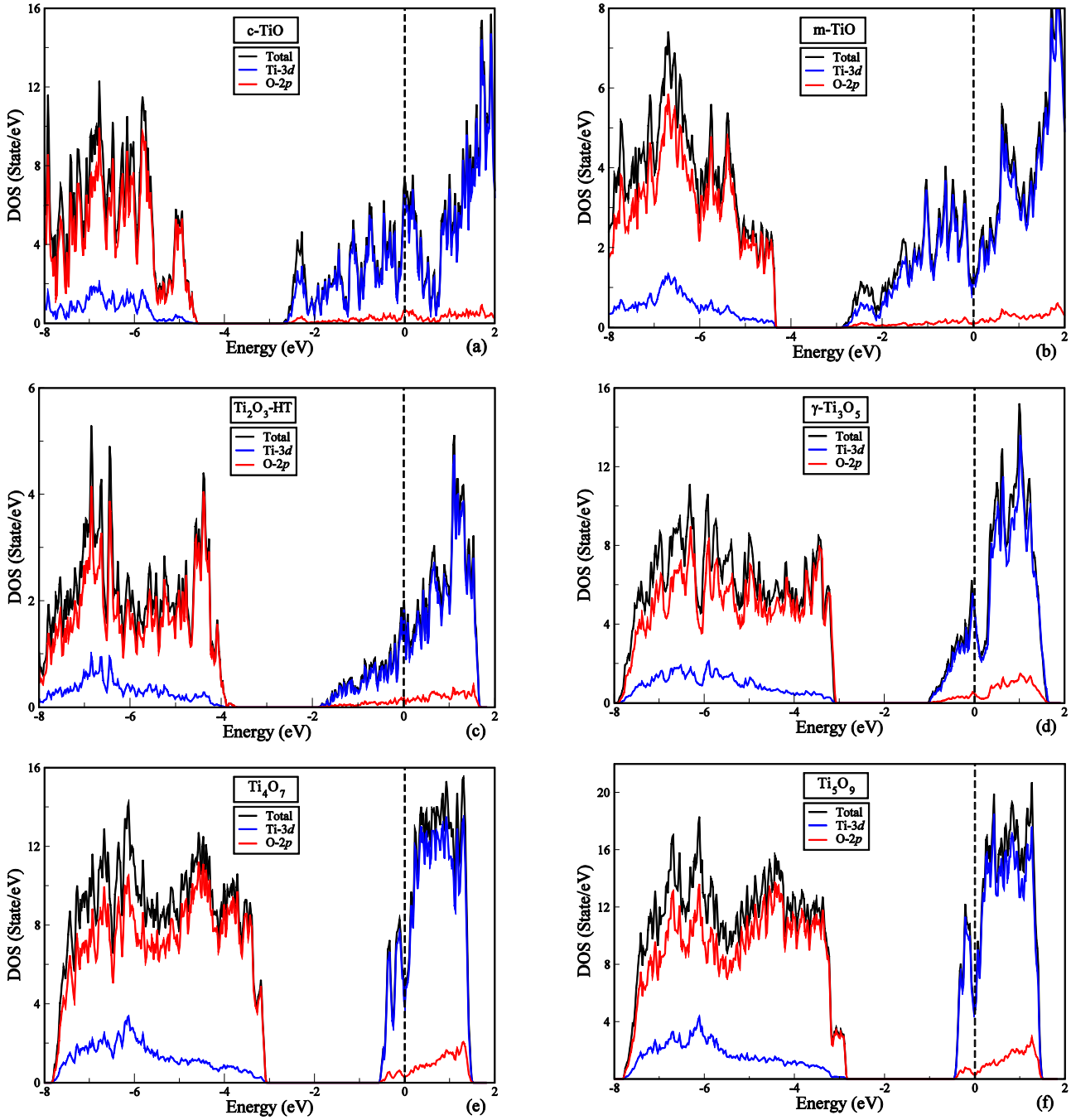

FIG. 3. Electronic densities of states for (a) c-TiO, (b) m-TiO, (c) Ti_2O_3-HT, (d) γ-Ti_3O_5, (e) Ti_4O_7, and (f) Ti_5O_9. The dashed line indicates the Fermi energy.

600 cm^{-1}. The highest isolated low-dispersion branch (located at 630–640 cm^{-1}) in Ti_5O_9 shows the vibrations of oxygen atoms both in plane and out of plane. These flat modes have a relatively small phonon relaxation time and group velocity, which usually hints for good heat insulating properties. In other words, the heat transport may "break down" when passing through these atoms. Nevertheless, less dispersive character of these branches implies high density of modes. This can affect the electron-phonon coupling, improving the superconducting properties of these compounds. Furthermore, phonon gaps with different magnitudes is observed in the Ti_nO_{2n-1} family except for Ti_2O_3-HT. The gap originates from the mass difference of Ti and O atoms, and its magnitude may differ depending on the average Ti–O bond length. This phonon gap is roughly located between ~300 and 400 cm^{-1} for c-TiO and m-TiO phases. Another phonon gap is also observed in the range of 550–600 cm^{-1} for the case of m-TiO, being located between two flat single modes. γ-Ti_3O_5 and Ti_4O_7 reveal quite narrow gaps placed at ~500 and 580 cm^{-1}, respectively. Yet another phonon gap appears in Ti_5O_9 in the frequency range ~610–630 cm^{-1}. In addition, from phonon-projected DOS of Ti_nO_{2n-1} ($n = 1$–5) it can be found out that the lower frequencies have stronger contribution of Ti whereas the higher frequencies are related to O atoms. As one moves

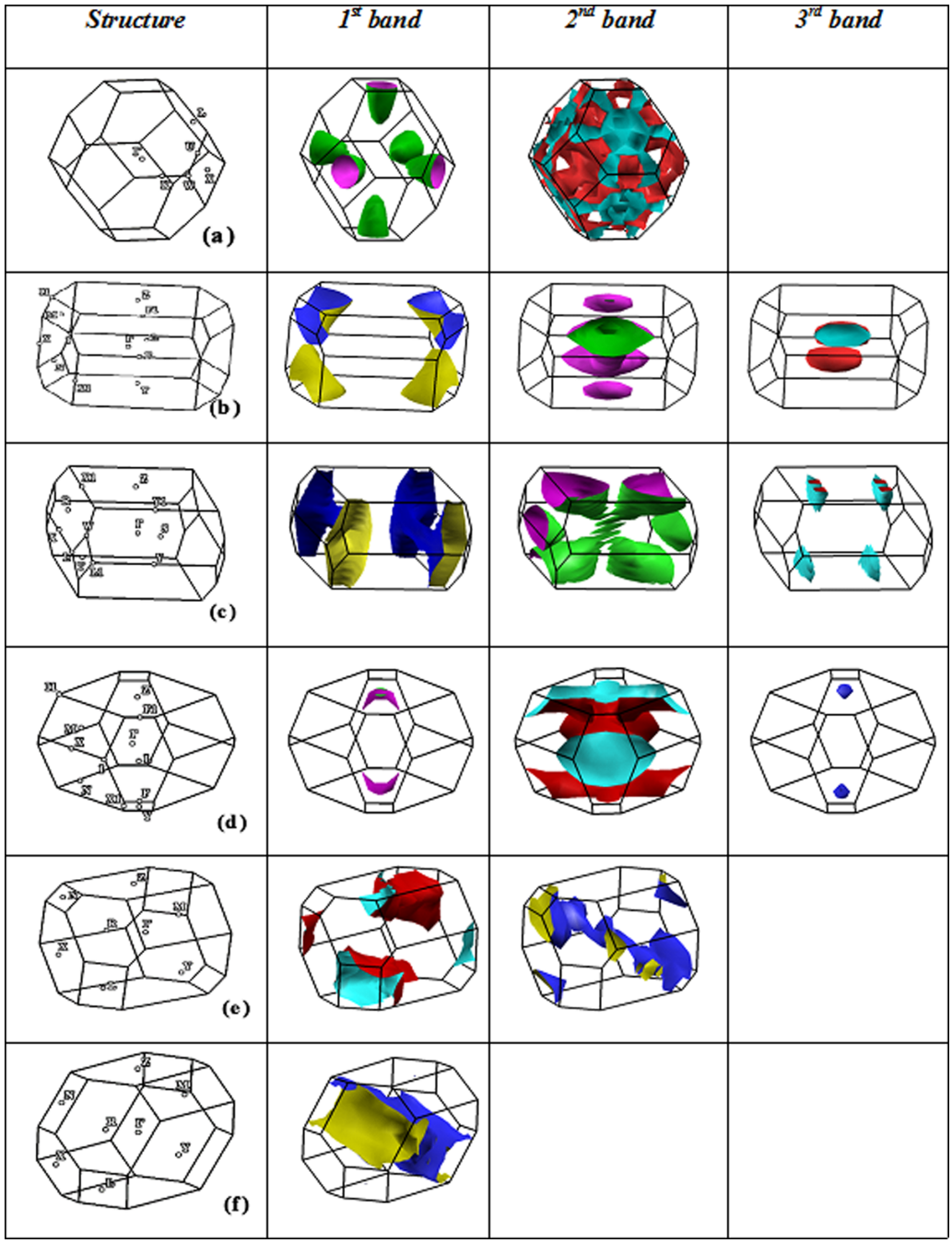

FIG. 4. The Fermi surface of (a) c-TiO, (b) m-TiO, (c) Ti_2O_3-HT, (d) γ-Ti_3O_5, (e) Ti_4O_7, and (f) Ti_5O_9. Each column corresponds to a band crossing the Fermi energy (numbered 1, 2, 3 in Fig. 2).

on from TiO to Ti_5O_9, the phonon couplings between Ti and O atoms get increased. The compounds with just few atoms per unit cell (c-TiO, m-TiO, Ti_2O_3-HT) are more "ordered" and their phonon DOS are more structured (revealing sharp peaks). However, this characteristic does not hold for the other ones. This might be merely an effect of "disordering" in the sense that there are more nonequivalent atom positions/bonds in these large unit-cell structures, corresponding to the wide and continuous peaks extended in the whole frequency ranges of phonon DOS. What is more, there is no band gap between acoustic and optical modes for all these structures. This suggests that the scattering of acoustic modes carrying heat can easily exchange phonon energy with optical modes (phonon-phonon interaction), thus resulting in low thermal conductivity in these compounds.

More explicitly, there are 14 atoms (7 Ti and 7 O) per unit cell for c-TiO, resulting in 42 independent normal modes. An outstanding softening is observed in LA mode along the Γ-L direction; see Fig. 5(a). Higher degeneracy of optical modes in the Γ point of c-TiO as compared to the other compounds reveals the higher symmetry of this structure.

The m-TiO includes 10 atoms (5 Ti and 5 O) in its unit cell, resulting in 30 normal modes. The acoustic modes of m-TiO [Fig. 5(b)] are more dispersed (up to $\sim$200 cm^{-1}) com-

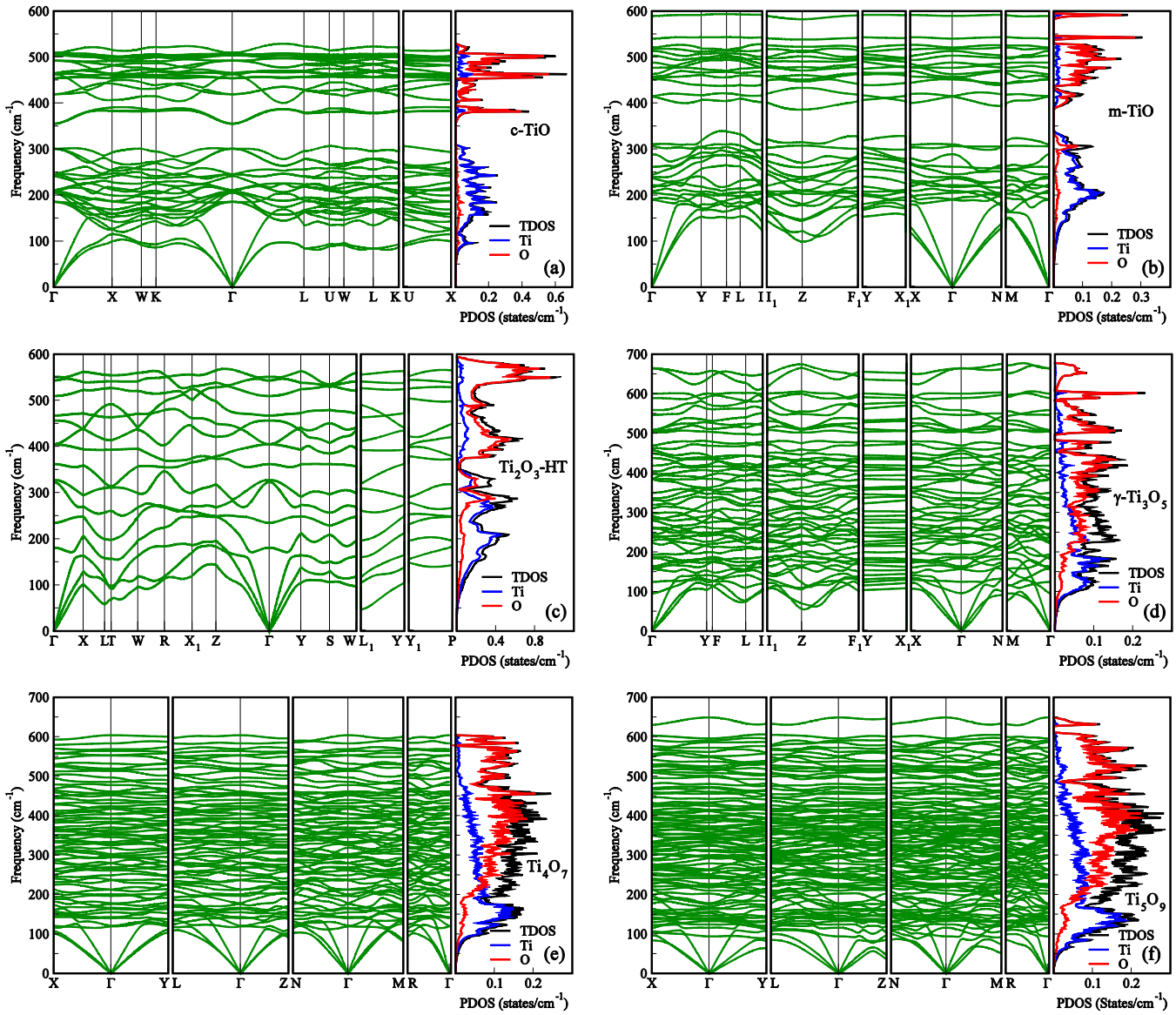

FIG. 5. The phonon dispersion curves and the corresponding phonon densities of states (resolved into Ti and O contributions) for (a) c-TiO, (b) m-TiO, (c) Ti_2O_3-HT, (d) γ-Ti_3O_5, (e) Ti_4O_7, and (f) Ti_5O_9.

pared to those of c-TiO, indicating stronger force constants. Higher stability of m-TiO versus c-TiO at low temperatures (less than ∼350 K) was also confirmed by calculating the free energy in our previous work [10]. In addition, the transverse acoustic (TA) modes of m-TiO are nondegenerate in all directions owing to its low symmetry. Moreover, m-TiO phonon dispersion curves [Fig. 5(b)] show a dip in acoustic branch along the I_1-Z-F_1 direction. In the Z point, Ti and O atoms vibrate in the same direction in the basal plane, while moving into F_1 point; Ti atoms have out-of-plane vibrations in counter phase. Ti_2O_3-HT has 5 atoms (2 Ti and 3 O) in its unit cell, yielding 15 normal modes. The corresponding phonon dispersion curves [Fig. 5(c)] make gapless manifold, differently from corundum-type Ti_2O_3-LT, whose physical properties are discussed in Appendix B. In Ti_2O_3-HT, the TA phonon frequencies at S and R points are higher than those of the T point. The former points are placed in the basal plane of BZ, whereas the latter one is out of this plane. Hence, it is expected that the phonon interaction is stronger in the basal plane that may lead to an anisotropic thermal conductivity. γ-Ti_3O_5, including 48 phonon branches, demonstrates a dip in the Z point of the phonon dispersion curves [Fig. 5(d)] similar to m-TiO. Both γ-Ti_3O_5 and m-TiO have the same symmetry group. A similar dip was also observed in the case of body-centered cubic metals by Savrasov *et al.* [49]. They have attributed this behavior to the intervention of the exp(i $\boldsymbol{q}$ ·$\boldsymbol{R}$) term and summing over lattice vectors $\boldsymbol{R}$ in the dynamical matrix. Furthermore, the noticeably flat bands extend also in the Y-X_1 direction.

C. Superconducting properties

Titanium suboxides Ti_nO_{2n-1} ($n = 1$–4) have been experimentally reported to be superconductors with T_C in the range of 1–8 K. Table II shows calculated results of electron-phonon properties of these materials. No experimental data

TABLE II. The calculated number of electrons averaged at Fermi surface $N(E_F)$, the electron-phonon coupling constant of titanium (λ_{Ti}), oxygen (λ_O) and their corresponding percentage contribution (%), total (λ_{eff}), isotope effect exponent (α), the logarithmically averaged phonon frequency ($\omega_{\log}$), and superconductivity transition temperature (T_c). These parameters are set using $\mu_{\text{eff}}{}^* = 0.16$.

	$N\ (E_F)$						T_C (K)	
Structure	(States/eV)	λ_{Ti}	λ_{O}	λ_{eff}	α	$\omega_{\log}$ (K)	This work	Expt.
c-TiO	55.53	0.68 (87.36%)	0.10 (12.64%)	0.78	0.40	271.7	7.4	1.0 [7], 5.5 [12], 7.4 [1]
m-TiO	35.41	0.47 (82.45%)	0.10 (17.55%)	0.57	0.27	335.5	2.8	1.0 [7], 2.3 [2]
Ti_2O_3-LT	11.98	0.09 (52.94%)	0.08 (47.06%)	0.17	−364.20	437.5	0.0	Nonsuperconductor [3]
Ti_2O_3-HT	15.90	0.78 (78.00%)	0.22 (22.00%)	1.00	0.42	266.3	13.6	8.0 [3]
γ-Ti_3O_5	51.10	0.46 (61.33%)	0.29 (38.67%)	0.75	0.37	328.3	8.0	7.1 [4]
Ti_4O_7	67.00	0.33 (57.89%)	0.24 (42.11%)	0.57	0.27	361.2	3.0	3.1 [4]
Ti_5O_9	73.17	0.37 (61.66%)	0.23 (38.44%)	0.60	0.29	310.2	3.5	Not found

were found for Ti_5O_9. So, our results serve as a prediction. For other compounds, the estimated T_C values are in good agreement with the experimental data. Therefore, it can be concluded that the presumed electron-phonon mechanism can indeed be responsible for superconductivity. The Ti_nO_{2n-1} ($n = 1$–5) materials reveal the electron-phonon coupling constant of less than 1. This suggests that they can be classified into intermediate regime. As the starting point to evaluate T_C, the semiempirical McMillan formula was used. As was mentioned earlier, the only uncertainty in the McMillan formula is the screened Coulomb pseudopotential ($\mu_c{}^*$), which is suggested to be 0.13 for transition metals [50].

Having set $\mu_c{}^* = 0.13$, we obtain T_C equal to 9.6, 4.5, 0.3, 16.9, 9.3, and 4.9 K for c-TiO, m-TiO, Ti_2O_3-LT, Ti_2O_3-HT, γ-Ti_3O_5, and Ti_4O_7 phases, respectively. Almost all these results are higher than the experimental values. One can note that these materials were reported to exhibit a paramagnetic phase in their metallic state [21,51,52]. Therefore, to have a better estimation of T_C for these structures, we considered a paramagnetic spin fluctuation (SF) within a phonon-mediated model. Our spin-polarized calculations showed a low magnetization ranging from 0.1 to 0.25 μ_B/Ti for these materials. The low magnetization of 0.23 μ_B/Ti obtained for Ti_4O_7 is consistent with paramagnetic phase of Ti_4O_7 calculated by Weissmann *et al.* [42]. These authors argue that the low value of magnetic moment (0.2 μ_B/Ti) and the presence of several quasidegenerate magnetic solutions would make Ti_4O_7 behave as a paramagnet due to temperature disorder. Therefore, taking into account the SF paramagnon superconductors, the McMillan formula can still be used and renormalized to [53]

$$T_c = \frac{\omega_{\log}}{1.2} \exp\left(-\frac{1.04\,(1+\lambda_{\text{eff}})}{\lambda_{\text{eff}} - \mu_{\text{eff}}{}^*\,(1+0.62\,\lambda_{\text{eff}})}\right), \qquad (9)$$

where $\lambda_{\text{eff}} = \lambda/(1+\lambda_{SF})$ (λ_{SF} denotes SF coupling constant) and $\mu_{\text{eff}}{}^* = (\mu_c{}^* + \lambda_{SF})/(1+\lambda_{SF})$ are effective electron-phonon coupling constant and the screened Coulomb pseudopotential, respectively. To enforce better agreement between our results and the experimental observations, we adjusted $\mu_{\text{eff}}{}^*$ to be 0.16 using $\mu_c{}^* = 0.13$ with λ_{SF} equal to 0.035. Intuitively, it implies that electron SF effect cannot coexist with electron-phonon coupling which may result in weakening the Cooper pairs in these structures. From Table II, it turns out that Ti atoms contribute more than O atoms in electron-phonon coupling. The higher T_C for c-TiO compared to m-TiO can be traced down to larger $N(E_F)$ and λ_{eff} of the former. According to Table II, the nonsuperconducting behavior was obtained for Ti_2O_3-LT, which agrees well with the experiment. In fact, the electron-phonon coupling is weak in Ti_2O_3-LT compared to the other compounds. In contrast, Ti_2O_3-HT shows an experimental value of T_C of about 8 K. However, our calculations predicted $T_C \sim 13.6$ K, which largely overestimates the experiment. We suggest that this discrepancy may arise from the defect sites in this structure. To investigate this, a $2 \times 2 \times 2$ supercell containing one oxygen vacancy atom was created. It resulted in a decrease of T_C by approximately 3 K. The details of calculation are provided in Appendix C. Comparing m-TiO, Ti_4O_7, and Ti_5O_9 with the other compounds shows that their coupling constants are rather weak. Hence, the possibility of having a high T_C is meager.

Moreover, using Eq. (14) in Ref. [54], isotope effect exponent (α) amounts to less than 0.5 for all these superconductors. For most of the monoatomic nontransition metals, the isotropic effect exponent is close to 0.5. Many other systems, on the other hand, deviate from this value. In particular, transition metals and alloys display values that are smaller than or equal to 0.5 [55]. Assuming that the electron-electron pairing interaction is mediated by phonons and neglecting the Coulomb repulsion between electrons, the BCS theory predicts the isotropic coefficient 0.5 or close to 0.5 for a monoatomic system. Therefore, the deviation is observed from BSC theory by considering the Coulomb repulsion. Such small value suggests that these materials are indeed conventional superconductors. In addition, the small value of α correlates with the low T_C in these compounds. For the case of

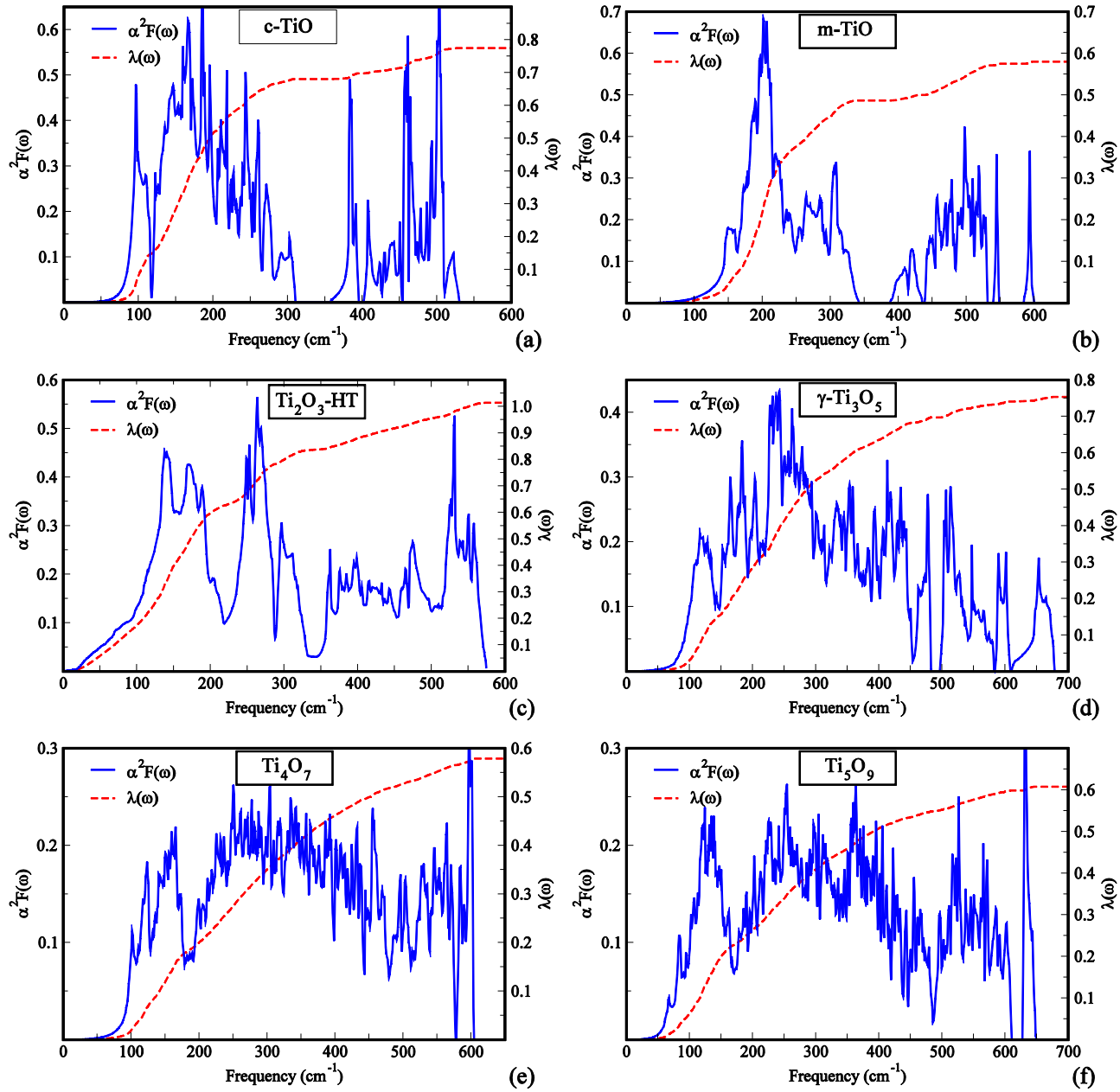

FIG. 6. The Eliashberg spectral function and electron-phonon coupling cosntant in Eqs. (6) and (7), respectively, for (a) c-TiO, (b) m-TiO, (c) Ti_2O_3-HT, (d) γ-Ti_3O_5, (e) Ti_4O_7, and (f) Ti_5O_9.

Ti_2O_3-LT having a large and negative value of α (also called inverse isotope exponent), the consequence is that T_C should not exceed $\sim$1 K [55].

Figure 6 depicts the corresponding $\alpha^2F(\omega)$ for Ti_nO_{2n-1} ($n = 1$–5) family. For the case of c-TiO, the number of prominent peaks observed in the low-frequency region (frequencies $<300\,cm^{-1}$) is larger than those in the high-frequency region (frequencies $>350\,cm^{-1}$). These peaks are mainly coming from Ti atom vibrations shown in the phonon projected DOS [Fig. 5(a)]. In m-TiO, there is an outstanding peak in $200\,cm^{-1}$ mostly due to the Ti optical modes, which provides the major contribution in the electron-phonon coupling. Turning to Ti_2O_3-HT and γ-Ti_3O_5, we find that the contribution of the peaks is related to regions in which Ti atoms play an important role in the vibrations. The Eliashberg spectral function for Ti_4O_7 and Ti_5O_9 is composed of low-intensity peaks resulting in a low electron-phonon coupling constant as compared to c-TiO, Ti_2O_3-HT, and γ-Ti_3O_5 structures. This might be a reason for the low T_C in Ti_4O_7 and Ti_5O_9 phases. Moreover (see Table II), at variance with the case of TiO and Ti_2O_3 in which the Ti vibrations dominate the coupling constant, in Ti_4O_7 and Ti_5O_9, the contribution of O vibrations is comparable with that of Ti vibrations. Due to the low symmetry of Ti_4O_7 and Ti_5O_9, more nonequivalent O atoms have contribution in the low-frequency regions of the phonon dispersion curves [shown in Figs 5(e) and 5(f)] compared to the TiO and Ti_2O_3 phases. Therefore, the denominator in Eq. (4) becomes smaller and λ_O gets larger. This could be a reason why O

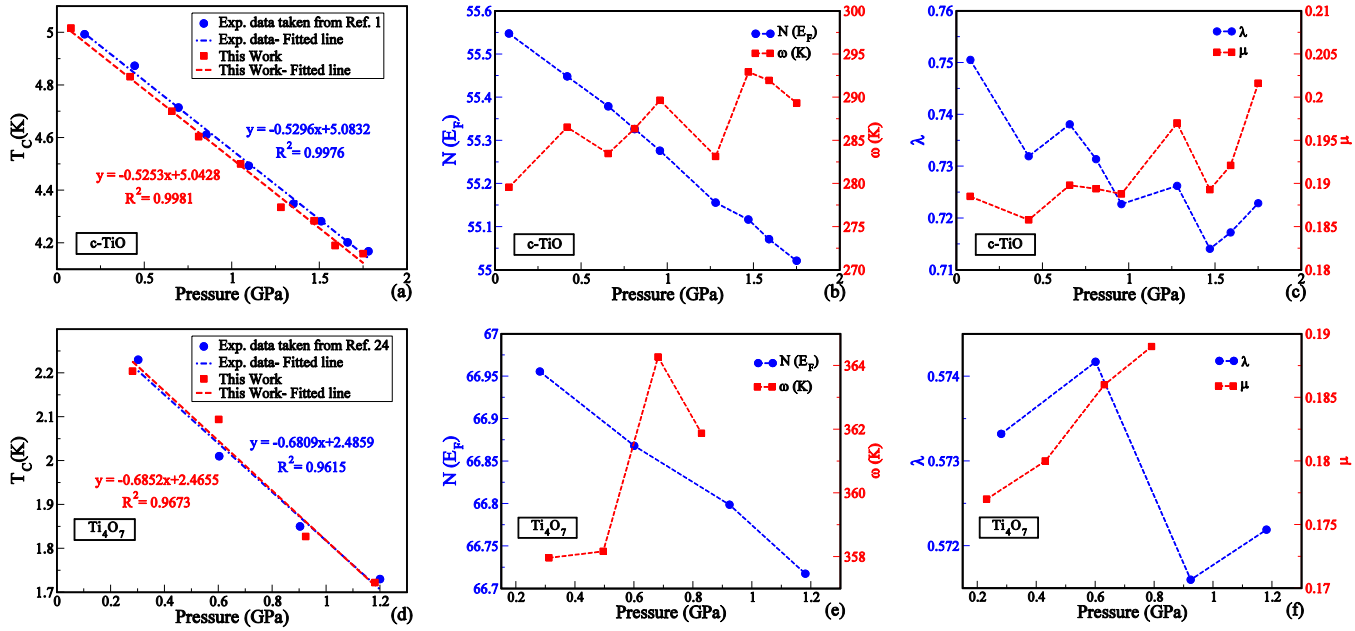

FIG. 7. The experimental T_C (K), number of Fermi electrons $N(E_F)$, average phonon frequency $\omega(K)$, electron-phonon coupling constant λ, and the screened Coulomb pseudopotential μ as a function of pressure (GPa) (upper panels: c-TiO, lower panels: Ti_4O_7).

atoms have more contributions in the electron-phonon coupling constant in Ti_4O_7 and Ti_5O_9 compared to TiO and Ti_2O_3 phases.

D. The influence of pressure on superconductivity

In this section, we offer some considerations reinforcing the proposed electron-phonon mechanism in superconductivity of Ti_nO_{2n-1} ($n = 1$–5). Recently, the influence of pressure on T_C of c-TiO [1] and Ti_4O_7 [24] has been experimentally reported. The decrease of T_C was observed by increasing the pressure at the rate of ∼0.7 and 0.5 K/GPa for c-TiO and Ti_4O_7, respectively. The similar trend follows from our calculations for both structures. It should be noted that the structures were relaxed in each pressure within the threshold of 0.01 GPa. However, the decrease rate of T_C was not the same as in experiment. The mismatch could occur due to fixing the parameter of $\mu_c{}^*$ independent of pressure. Logically, when the material is under positive or negative pressure, the orbital interactions change. Hence, the electron-electron Coulomb interaction should be altered. Therefore, it is needed to adjust the parameter of $\mu_c{}^*$ in the presence of pressure. By tuning this parameter, the decrease rate of T_C could be made more consistent with experiment.

Figure 7 illustrates the behavior of T_C and superconducting quantities versus pressure for both c-TiO and Ti_4O_7 phases. The experimental behavior of T_C with respect to pressure seems almost linear for both structures. The relevant superconducting parameters in conventional superconductors are linked in a relation known as the McMillan-Hopfield parameter defined as $\lambda_{\text{eff}} = \frac{N_F\langle I^2\rangle}{M\langle\omega^2\rangle}$, where $\langle I^2\rangle$ is the electron-phonon matrix element averaged over the Fermi sea [56]. The denominator arises from the lattice phonons, M is ion mass, and $\langle\omega^2\rangle$ is the average phonon frequency squared. As seen from Fig. 7, $N(E_F)$ is decreased by increasing the pressure. Moreover, the average phonon frequency [as shown in Figs. 7(b) and 7(e)] is increased but not monotonously. Consequently, it is expected that λ_{eff} would decrease by increasing the pressure [Figs. 7(c) and 7(f)], which may result in a decrease of T_C. Meanwhile, there is no well-defined behavior explaining the variation of electron-phonon coupling constant (nonuniform decrease) and the screened Coulomb pseudopotential (nonuniform increase) versus pressure. This nonuniformity is observed for electron-phonon coupling of hydrogen sulfide substituted with different group VI- and V concentration for sulfur [57]. In fact, the variation of T_C with the pressure is a complex function of λ, $\mu_c{}^*$, and $N_F\langle I^2\rangle$, as is discussed in Appendix D. In summary, the agreement between our results and the experiment highlights that the electron-phonon interaction accounts for the superconductivity mechanism in these structures.

IV. CONCLUSIONS

In the present work, the electronic and phonon structures along with the electron-phonon interaction were discussed for titanium suboxides c-TiO, m-TiO, Ti_2O_3-LT, Ti_2O_3-HT, γ-Ti_3O_5, Ti_4O_7, and Ti_5O_9 on the basis of density-functional (perturbation) calculations. The electronic results revealed that these structures are metallic with rather highly mobile electrons and extremely flat bands around the Fermi level that seems to provide prerequisites for superconductivity in these materials. The phonon-mediated mechanism along with paramagnetic spin fluctuation model was proposed to refine the electron-phonon interaction picture in these materials. The proposed model was able to predict the T_C of Ti_nO_{2n-1} ($n = 1$–4) in good agreement with the corresponding experimental values.

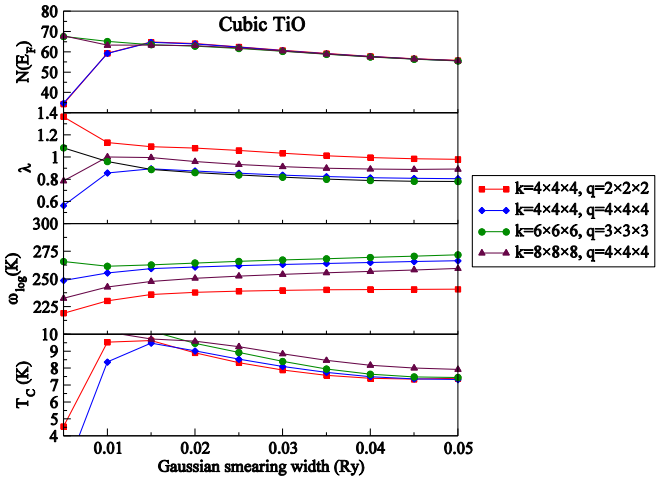

FIG. 8. The calculated number of electrons averaged at Fermi surface $N(E_F)$, the electron-phonon coupling constant λ, the logarithmically averaged phonon frequency $\omega_{\log}$, and superconductivity transition temperature T_C at $\mu_{\text{eff}}{}^* = 0.16$ as a function of the Gaussian smearing width (δ), with k-point mesh of $4 \times 4 \times 4$, $6 \times 6 \times 6$, and $8 \times 8 \times 8$ and phonon q-point mesh of $2 \times 2 \times 2$, $3 \times 3 \times 3$, and $4 \times 4 \times 4$ for c-TiO.

Low T_C of these materials can be attributed to the low value of electron-phonon coupling constant. The major contribution to electron-phonon coupling constant of Ti_nO_{2n-1} ($n = 1$–4) comes from Ti atoms. By means of this model, the $T_C \sim 3.5$ K was predicted for Ti_5O_9, a second Magnéli phase of titanium suboxide family. Based on the obtained results, titanium suboxides Ti_nO_{2n-1} ($n = 1$–5) can be classified as materials revealing a weak coupling regime. Furthermore, this model can explain the variations of experimental T_C of c-TiO and Ti_4O_7 with respect to pressure. By increasing the pressure, the number of electrons in the Fermi level decreases and the average optical phonon frequencies are shifted upwards, which results in a decrease of electron-phonon coupling constant in these structures.

TABLE III. The electron-phonon properties of the defected Ti_2O_3-HT. These parameters are set using $\mu_{\text{eff}}{}^* = 0.16$ for Ti_2O_3-HT including one oxygen vacancy.

	$N(E_F)$			T_C (K)	
Structure	(states/eV)	λ_{eff}	$\omega_{\log}$ (K)	This work	Expt.
Defected Ti_2O_3-HT	55.53	0.85	288.4	10.2	8.4 [1]

ACKNOWLEDGMENTS

Partial financial support by the Research Council of the University of Tehran is acknowledged. The computation in this work was partially performed using the facilities of the Center for Information Science in JAIST. Also, the authors thank Andrei Postnikov from Université de Lorraine (LCP-A2MC) for careful reading, useful discussions, valuable hints, and comments.

APPENDIX A: ELECTRON-PHONON PROPERTIES: CONVERGENCE CRITERIA

Figure 8 shows the calculated number of electrons averaged at the Fermi surface $N(E_F)$, the electron-phonon coupling constant (λ), the logarithmically averaged phonon frequency ($\omega_{\log}$), and the superconductivity transition temperature (T_c) at $\mu_{\text{eff}}{}^* = 0.16$ as a function of the Gaussian smearing width δ in Eq. (6) (as a replacement of delta funtion) for c-TiO as a typical example of titanium suboxides materials. The calculations are performed in different electronic k mesh and phonon q mesh to achieve almost a certain convergence.

As it can be seen, the convergence is almost achieved for the electron-phonon properties in $6 \times 6 \times 6$ and $3 \times 3 \times 3$ k and q mesh with Gaussian smearing parameter of 0.05 Ry.

APPENDIX B: ELECTRONIC, PHONON, AND ELECTRON-PHONON PROPERTIES OF Ti_2O_3-LT

The electronic band structure and electronic DOS of Ti_2O_3-LT are presented in Fig. 9. The results of electronic DOS is in a good agreement with those by Andersson *et al.* [58].

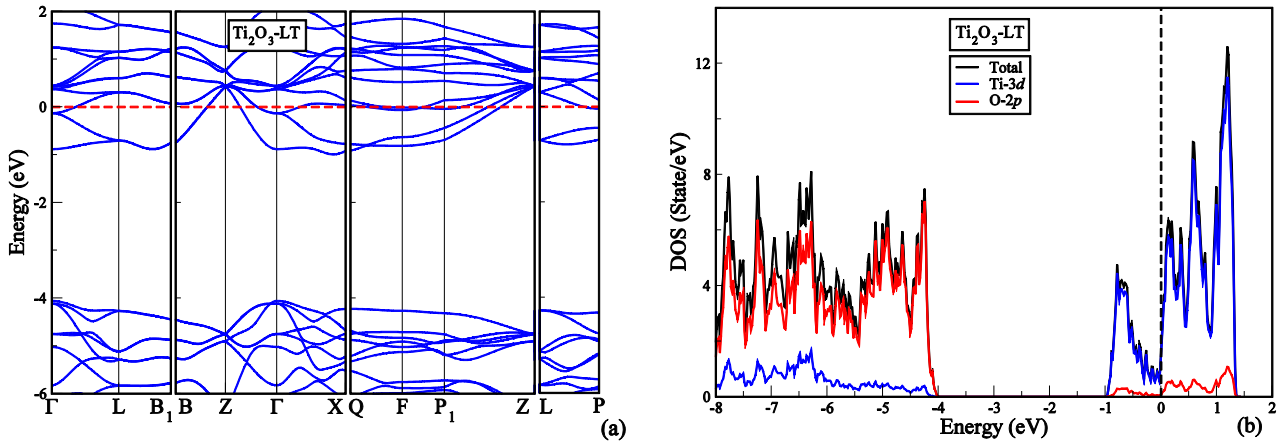

FIG. 9. The electronic and corresponding density of states for Ti_2O_3-LT.

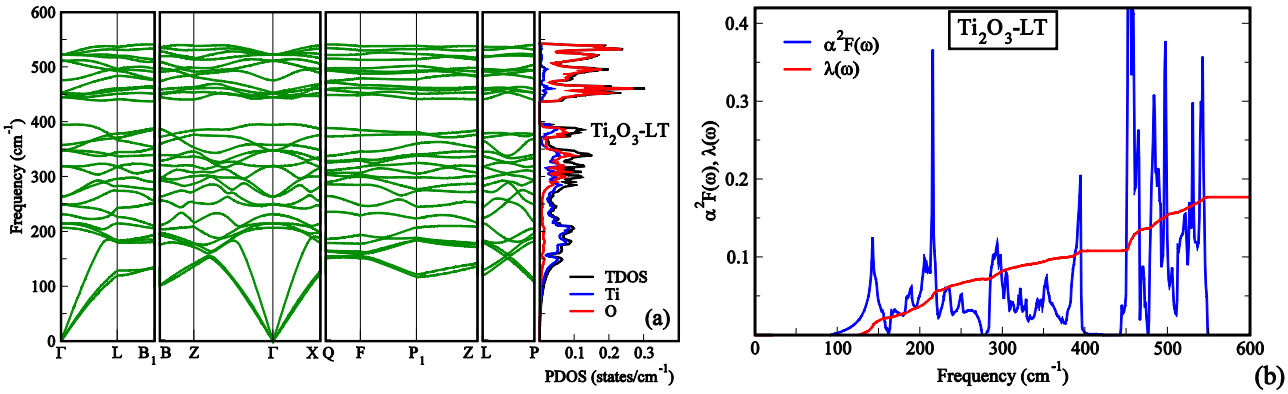

FIG. 10. (a) phonon dispersion and (b) Eliashberg spectral function for Ti_2O_3-LT.

The observation of flat and steep bands in Fermi level can suggest this structure as a potential candidate for superconductivity, albeit, this property is not solely responsible for superconductivity of the materials. The dynamical stability and the Eliashberg spectral function are represented in Fig. 10.

As observed in Fig. 10(a), the lower-frequency region is composed of Ti vibrations (less than 250 cm^{-1}). In the intermediate range of frequencies (280–400 cm^{-1}), the coupling between Ti and O modes is observed. The higher-frequency region (over 450 cm^{-1}) comes from O atom vibrations which make dispersionless branches. The phonon gap is observed at frequecy ranges ∼400–440 cm^{-1}. Figure 10(b) shows that higher frequencies contribute more to the electron-phonon interactions by enhancing the denominator of Eq. (7), resulting in a very low electron-phonon coupling constant. This fact prevents this structure from showing a superconductivity behavior, in contrast to Ti_2O_3-HT.

APPENDIX C: INFLUENCE OF OXYGEN VACANY ON SUPERCODUCTING TRANSITION TEMPRETURE OF Ti_2O_3-HT

To resolve the available inconsistency between our calculated and experimental data for T_C in Ti_2O_3-HT, as depicted in Table II, the presence of oxygen vacancy was considered in the structure. As mentioned earlier, the Ti_2O_3 phase can persist throughout $TiO_{1.49}$ to $TiO_{1.51}$ [35]. Therefore, a $2 \times 2 \times 2$ supercell was created from this structure and one oxygen atom was removed in a way as to keep the symmetry. The phonon dispersion curve and the Eliashberg spectral function are depicted in Fig. 11.

The defected Ti_2O_3-HT consists of 16 Ti and 23 O atoms in the unit cell, yielding 117 modes, as shown in Fig. 11(a). The phonon dispersion curve acknowleges the dynamical stability of this structure. The electron-phonon properties of Ti_2O_3-HT including one oxygen vacancy are shown in Table III.

According to Table III, the oxygen vacancy weakens electron-phonon coupling constant [as displayed in Fig. 11(b)] compared to that of pure Ti_2O_3-HT. This may result in lower T_C compared to the pure one, closer to the experimental value. It should be noted that a better result may be obtained by extending the supercell to include the proper oxygen vacancy concentration.

APPENDIX D: THE INFLUENCE OF PRESSURE ON SUPERCONDUCTING TEMPERATURE

The shift in T_C under pressure is mainly caused by changes in E_F [or $N(E_F)$] and volume (V) (the electron-phonon interaction in the lattice), which can be expressed as a chain rule of these quantities [59] :

$$\frac{dT_C}{dP} \approx \frac{\partial T_C}{\partial E_F}\frac{dE_F}{dP} + \frac{\partial T_C}{\partial V}\frac{dV}{dP}. \tag{D1}$$

Taking logarithm from both sides of the McMillan formula in Eq. (5), using expressions such as bulk modulus, $B = -V\frac{\partial P}{\partial V}$, Grüneisen parameter, $\gamma = -\frac{d\ \ln\omega}{d\ \ln V}$, the mean squared of electron-phonon matrix elements, $\eta = N_F\langle I^2\rangle$, and

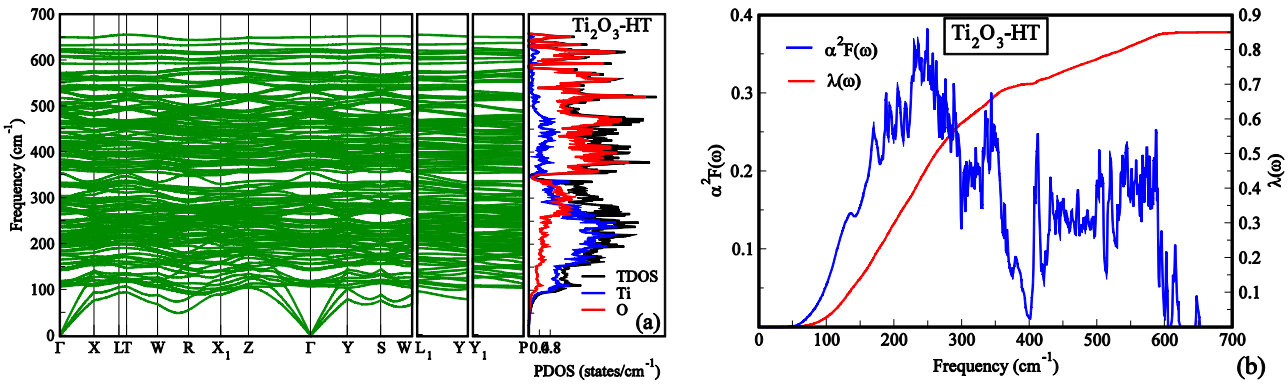

FIG. 11. (a) The phonon dispersion curve and (b) the Eliashberg spectral function for Ti_2O_3-HT including oxygen vacancy.

introducing these expressions into (D1), after a few tedious but straightforward manipulations one obtains

$$\frac{d\ln T_C}{dP} \approx \frac{1}{B}\left\{\gamma + \left[\frac{1.04\lambda}{\lambda - \mu_c^*(1+0.62\lambda)} - \frac{1.04\lambda(1+\lambda)(1-0.62\lambda)}{[\lambda - \mu_c^*(1+0.62\lambda)]^2}\right]\left[2\gamma + \frac{d\ln\eta}{d\ln V}\right]\right\}. \tag{D2}$$

The equation above holds, if μ_c^* is considered to be independent of the pressure.

[1] C. Zhang, F. X. Hao, G. Y. Gao, X. Liu, C. Ma, Y. Lin, Y. W. Yin, and X. G. Li, npj Quantum Mater. **2**, 2 (2017).
[2] N. Doyle, J. Hulm, C. Jones, R. Miller, and A. Taylor, Phys. Lett. A **26**, 604 (1968).
[3] Y. Li, Y. Weng, J. Zhang, J. Ding, Y. Zhu, Q. Wang, Y. Yang, Y. Cheng, Q. Zhang, P. Li, and J. Lin, NPG Asia Mater. **10**, 522 (2018).
[4] K. Yoshimatsu, O. Sakata, and A. Ohtomo, Sci. Rep. **7**, 12544 (2017).
[5] A. Manthiram, J. Swinnea, Z. Sui, H. Steinfink, and J. Goodenough, J. Am. Chem. Soc. **109**, 6667 (1987).
[6] Y. Mizuguchi, K. Deguchi, S. Tsuda, T. Yamaguchi, H. Takeya, H. Kumakura, and Y. Takano, Appl. Phys. Express **2**, 083004 (2009).
[7] J. Hulm, C. Jones, R. Hein, and J. Gibson, J. Low Temp. Phys. **7**, 291 (1972).
[8] M. Banus, T. Reed, and A. Strauss, Phys. Rev. B **5**, 2775 (1972).
[9] D. Watanabe, J. Castles, A. Jostsons, and A. Malin, Acta Crystallogr. **23**, 307 (1967).
[10] S. V. Hosseini, M. Abbasnejad, and M. R. Mohammadizadeh, arXiv:2110.12267.
[11] S. P. Denker, J. Appl. Phys. **37**, 142 (1966).
[12] D. Wang, C. Huang, J. He, X. Che, H. Zhang, and F. Huang, ACS Omega **2**, 1036 (2017).
[13] J. Xu, D. Wang, H. Yao, K. Bu, J. Pan, J. He, F. Xu, Z. Hong, X. Chen, and F. Huang, Adv. Mater. **30**, 1706240 (2018).
[14] M. Onoda, J. Solid State Chem. **136**, 67 (1998).
[15] S. Åsbrink and A. Magnéli, Acta Crystallogr. **12**, 575 (1959).
[16] S.-H. Hong and S. Åsbrink, Acta Crystallogr. Sect. B: Struct. Crystallogr. Cryst. Chem. **38**, 2570 (1982).
[17] A. Padilha, J. M. Osorio-Guillén, A. Rocha, and G. M. Dalpian, Phys. Rev. B **90**, 035213 (2014).
[18] K. Kobayashi, M. Taguchi, M. Kobata, K. Tanaka, H. Tokoro, H. Daimon, T. Okane, H. Yamagami, E. Ikenaga, and S. I. Ohkoshi, Phys. Rev. B **95**, 085133 (2017).
[19] M. Marezio, D. McWhan, P. Dernier, and J. Remeika, J. Solid State Chem. **6**, 213 (1973).
[20] D. Kaplan, C. Schlenker, and J. Since, Philos. Mag. **36**, 1275 (1977).
[21] L. Mulay and W. Danley, J. Appl. Phys. **41**, 877 (1970).
[22] M. Abbate, R. Potze, G. Sawatzky, C. Schlenker, H. Lin, L. Tjeng, C. Chen, D. Teehan, and T. Turner, Phys. Rev. B **51**, 10150 (1995).
[23] B. Chakraverty, J. Phys. Lett. **40**, 99 (1979).
[24] S. Sekiguchi, T. Shiraishi, K. Miura, C. Kawashima, K. Yoshimatsu, A. Ohtomo, H. Kamioka, and H. Takahashi, J. Phys. Soc. Jpn. **88**, 035001 (2019).
[25] F. Giustino, Rev. Mod. Phys. **89**, 015003 (2017).
[26] W. McMillan, Phys. Rev. **167**, 331 (1968).
[27] P. B. Allen and R. Dynes, Phys. Rev. B **12**, 905 (1975).
[28] T. Koretsune and R. Arita, Comput. Phys. Commun. **220**, 239 (2017).
[29] P. Giannozzi, S. Baroni, N. Bonini, M. Calandra, R. Car, C. Cavazzoni, D. Ceresoli, G. L. Chiarotti, M. Cococcioni, I. Dabo, and A. Dal Corso, J. Phys.: Condens. Matter **21**, 395502 (2009).
[30] J. P. Perdew, K. Burke, and M. Ernzerhof, Phys. Rev. Lett. **77**, 3865 (1996).
[31] H. J. Monkhorst and J. D. Pack, Phys. Rev. B **13**, 5188 (1976).
[32] W. R. Robinson, J. Solid State Chem. **9**, 255 (1974).
[33] Z. Shen, Q. Shi, W. Huang, B. Huang, M. Wang, J. Gao, Y. Shi, and T. Lu, Appl. Phys. Lett. **111**, 191902 (2017).
[34] S. Andersson, D. Templeton, S. Rundqvist, E. Varde, and G. Westin, Acta Chem. Scand. **14**, 1161 (1960).
[35] B. Xu, H. Y. Sohn, Y. Mohassab, and Y. Lan, RSC Adv. **6**, 79706 (2016).
[36] S. Abrahams, Phys. Rev. **130**, 2230 (1963).
[37] W. Setyawan and S. Curtarolo, Comput. Mater. Sci. **49**, 299 (2010).
[38] V. Ern and A. Switendick, Phys. Rev. **137**, A1927 (1965).
[39] J. Graciani, A. Márquez, and J. F. Sanz, Phys. Rev. B **72**, 054117 (2005).
[40] Y. Pan, Y. Li, Q. Zheng, and Y. Xu, J. Alloys Compd. **786**, 621 (2019).
[41] J. Kim and S. Kang, J. Mater. Chem. A **2**, 2641 (2014).
[42] M. Weissmann and R. Weht, Phys. Rev. B **84**, 144419 (2011).
[43] I. Slipukhina and M. Ležaić, Phys. Rev. B **90**, 155133 (2014).
[44] J. Noffsinger, F. Giustino, S. G. Louie, and M. L. Cohen, Phys. Rev. B **77**, 180507 (2008).
[45] M. Johannes and I. Mazin, Phys. Rev. B **77**, 165135 (2008).
[46] U. Argaman, R. E. Abutbul, Y. Golan, and G. Makov, Phys. Rev. B **100**, 054104 (2019).
[47] M. T. Dove, Am. Mineral. **82**, 213 (1997).
[48] A. Togo, L. Chaput, I. Tanaka, and G. Hug, Phys. Rev. B **81**, 174301 (2010).
[49] S. Y. Savrasov and D. Y. Savrasov, Phys. Rev. B **54**, 16487 (1996).
[50] B. M. Klein and D. A. Papaconstantopoulos, Phys. Rev. Lett. **32**, 1193 (1974).
[51] L. Van Zandt, J. Honig, and J. Goodenough, J. Appl. Phys. **39**, 594 (1968).
[52] S.-i. Ohkoshi, Y. Tsunobuchi, T. Matsuda, K. Hashimoto, A. Namai, F. Hakoe, and H. Tokoro, Nat. Chem. **2**, 539 (2010).
[53] B. Wiendlocha, J. Tobola, M. Sternik, S. Kaprzyk, K. Parlinski, and A. Oleś, Phys. Rev. B **78**, 060507 (2008).

[54] S. Jain and C. Kachhava, Phys. Status Solidi B **101**, 619 (1980).
[55] V. V. Kresin and W. Knight, in *Pair Correlations in Many-Fermion Systems*, edited by V. Z. Kresin (Plenum, New York, 1998), p. 245.
[56] L. W. Nixon, D. Papaconstantopoulos, and M. J. Mehl, Phys. Rev. B **76**, 134512 (2007).
[57] Y. Ge, F. Zhang, and Y. Yao, Phys. Rev. B **93**, 224513 (2016).
[58] D. A. Andersson, P. A. Korzhavyi, and B. Johansson, Phys. Rev. B **71**, 144101 (2005).
[59] S. Huang, C. Chu, F. Fradin, and L. Welsh, Solid State Commun. **16**, 409 (1975).